chemistry

MDPI

Review

Hydrogen Evolution upon Ammonia Borane Solvolysis: Comparison between the Hydrolysis and Methanolysis Reactions

Naixin Kang [1], Changlong Wang [2,*] and Didier Astruc [1,*]

[1] ISM, UMR CNRS N°5255, University of Bordeaux, 33405 Talence CEDEX, France
[2] Institute of Circular Economy, Faculty of Materials and Manufacturing, Beijing University of Technology, Beijing 100124, China
* Correspondence: changlongwang1987@gmail.com (C.W.); didier.astruc@u-bordeaux.fr (D.A.)

Abstract: Hydrogen (H_2) production is a key challenge for green carbon-free sustainable energy. Among the H_2 evolution methods from H-rich materials, ammonia borane (AB) solvolysis stands as a privileged source under ambient and sub-ambient conditions given its stability, non-toxicity, and solubility in protic solvents, provided suitable and optimized nanocatalysts are used. In this paper dedicated to Prof. Avelino Corma, we comparatively review AB hydrolysis and alcoholysis (mostly methanolysis) in terms of nanocatalyst performances and discuss the advantages and inconveniences of these two AB solvolysis methods including AB regeneration.

Keywords: ammonia borane; hydrogen (H_2); hydrolysis; methanolysis; nanocatalyst

Citation: Kang, N.; Wang, C.; Astruc, D. Hydrogen Evolution upon Ammonia Borane Solvolysis: Comparison between the Hydrolysis and Methanolysis Reactions. *Chemistry* **2023**, *5*, 886–899. https://doi.org/10.3390/chemistry5020060

Academic Editors: José Antonio Odriozola, Hermenegildo García and Edwin Charles Constable

Received: 5 February 2023
Revised: 20 March 2023
Accepted: 7 April 2023
Published: 13 April 2023

1. Introduction

Hydrogen (H_2) generation is one of the main focuses of current research, particularly because it is a green energy source toward the replacement of harmful fossil-based fuel [1,2]. H_2 energy has appeared to be essential, because it is carbon-free, without pollution, and it involves an excellent energy storage density [1]. Besides water (hydrogen evolution reaction, HER [3]), liquid-phase hydrogen generation systems include a variety of metal borohydrides, ammonia and its borane derivatives (ammonia borane, amine boranes, hydrazine borane, etc.), formic acid, and several hydrocarbons [1]. Among all these possibilities, since the seminal work by Chandra and Xu [4], ammonia borane (AB) has appeared to be by far the most studied H_2 source. During the first decade of the century, AB thermolysis was the subject of various studies [5,6], but the high temperatures required (only 15% H_2 is obtained at 200 °C [7]), long induction times, and ill-defined mixture of B_xN_y derivatives obtained made nanocatalyzed AB solvolysis a privileged route [2,4–23]. Therefore, we are briefly reviewing here the two major AB solvolysis routes, i.e., hydrolysis and methanolysis, with the goal of comparing them, because, despite similarities, there are important differences in terms of environmental concern, rates, efficiencies, facilities, and side reactions. Publications generally focus on either of them without comparison with the alternative solvolysis method. In conclusion, researchers should be able to consider the parameters and state of the art toward selecting their choice. Finally, in the conclusion, prospects are formulated toward improving the hydrogen generation process upon AB solvolysis.

2. Ammonia Borane (AB)

Ammonia borane, currently abbreviated as AB, is a white solid, due to the intermolecular H bonding (NH—HB distance about 2 Å [24]). Its molecular weight M_w is 30.8 g·mol^{-1} and its density at 25 °C is ρ = 0.78 g·mL^{-1}. It is stable in water at neutral pH, whereas $NaBH_4$, another H_2 source, slowly reacts with water. AB is stabilized, formally by a dative

bond from N to B with a net electron transfer from N to B (Figure 1, left) of approximately 0.5 electrons and with the formation of a compound that is 65% ionic; the ionic structure is represented on the right of Figure 1 [25]. Thus, the N-H bonds are acidic, whereas the B-H bonds are hydridic.

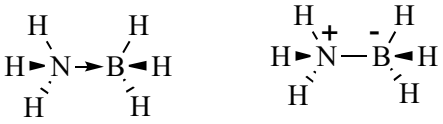

Figure 1. Bonding in NH_3BH_3.

AB is soluble in ether, 1,2-dimethoxyethane (DME), water, alcohols, and many ionic liquids; slightly soluble in benzene, dichloromethane, and chloroform; insoluble in alkanes.

AB was first synthesized by Shore and Parry and reported in 1955 (Equation (1)) [26].

$$LiBH_4 + NH_4Cl \rightarrow NH_3BH_3 + LiCl + H_2 \quad (1)$$

Since then, many variations of this commonly utilized metathesis-type synthesis between metal borohydrides MBH_4 and ammonium salts NH_4X have appeared, summarized six decades later in Shore's review [27].

The synthesis of AB was improved by the use of methyl borate, $B(OMe)_3$ [28]. Methyl borate had indeed long been available from boric acid, $B(OH)_3$, and methanol, a reaction reported in 1953 by Schlesinger et al. (Equation (2)) [29].

$$H_3BO_3 + 4CH_3OH \rightarrow B(OMe)_3 + MeOH + 3H_2O \quad (2)$$

In particular, Ramachandran's group developed this especially practical synthesis from $B(OMe)_3$ using $LiAlH_4$ in THF added to a mixture of $B(OMe)_3$ and NH_4Cl in THF at 0 °C over 1 h, followed by stirring 3 h at 0 °C (90% isolated yield after extraction with ether) (Equation (3)) [30].

$$B(OMe)_3 + NH_4Cl \xrightarrow[\text{THF, 0 °C, 3 h}]{LiAlH_4} BH_3NH_3 + Al(OMe)_3 + LiCl + H_2 \quad (3)$$

In 2015, Ramachandran's group even reported an astute extension of the metathesis reaction of Equation (1) to the syntheses of a variety of amine borane derivatives in high yields and purity by reactions of alkylammonium sulfate derivatives with $NaBH_4$ [29].

3. H_2 Generation upon AB Hydrolysis

Besides properties such as a mild reducing agent and other properties that are reviewed elsewhere [2,5,6], AB is an excellent source of H_2, which is due to its low molecular weight, high hydrogen content (19.6 wt%), high solubility in water (35 g of AB for 100 g of water), stability, and lack of toxicity.

3.1. Use of an Acidic Medium

Although AB is stable in neutral or slightly basic aqueous solution, H_2 is formed in acidic solutions owing to the hydricity [31] of the BH groups of AB. Chandra and Xu reported that 3 mol H_2 was released from AB in aqueous solution in the presence of solid acids such as Dorex, Amberlyst, and Nafion-H, in a few minutes under ambient conditions, according to Equation (4) [31]. CO_2 also reacts as an acid, upon dissolution into water, releasing H_2 together with the formation of boric acid [32].

$$NH_3BH_3 + 2H_2O \xrightarrow{H^+} NH_4^+, BO_2^- + 3H_2 \quad (4)$$

3.2. Use of a Transition-Metal Catalyst

In neutral aqueous medium, the presence of a transition-metal-based catalyst is necessary to achieve AB hydrolysis with the formation of 3 mol H_2 and hydrated ammonium borate (Equation (5)).

$$NH_3BH_3 + 4H_2O \xrightarrow{\text{metal-based catalyst}} NH_4^+, B(OH)_4^- + 3H_2 \quad (5)$$

A large variety of transition-metal-based catalysts including homogeneous and heterogeneous catalysts, transition-metal complexes, oxides, transition-metal nanoparticles (NPs), and heterobinuclear catalysts have been reported and reviewed by Xu's group and others [1–23]. Ramachandran's group reported that upon catalysis with $RuCl_3$, NH_3 was also produced along with H_2 evolution during AB hydrolysis, and the amount of NH_3 produced increased upon increasing the AB concentration, which would be a problem for the realization of fuel cells. The setup for H_2 production from AB and measurement is shown in Figure 2 [33].

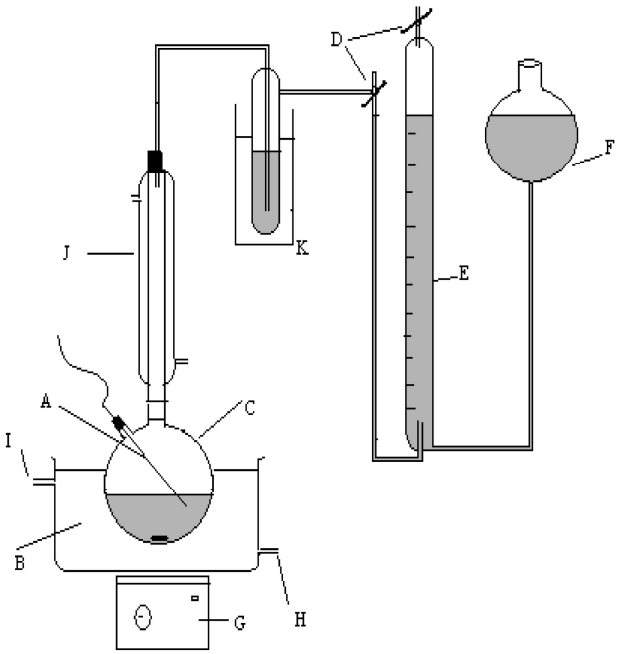

Figure 2. Setup for the measurement of evolved H_2: (A) thermocouple, (B) bath temperature, (C) round-bottom flask, (D) stop cock, (E) gas burette, (F) leveling flask, (G) magnetic stirrer, (H) water inlet, (I) water outlet, (J) reflux condenser, and (K) water trap. Reproduced with permission from Ref. [32]. Copyright 2007 American Chemical Society.

These authors also found that the borate produced in the reaction of Equation (5) was ammonium tetraborate $\{[(NH)_4]_2[B_4O_5(OH)_4]\cdot 1.41H_2O\}$ with the nature of the borate anions depending on the pH, and polyborate anions being formed at higher pH [32]. In early studies, transition-metal complexes were shown to be efficient for AB hydrolysis with H_2 evolution. Mechanistic studies privileged both B-H and N-H cleavage in the rate-determining step (RDS) [33,34]. The intermediacy of organometallic or inorganic radicals during the catalyst process might play a significant role [35]. Other studies with molybdenum complexes showed that the mechanism depended on the oxidation state of the catalyst [36]. Finally, with Co-Ni and Ni NPs, O-H activation by the catalyst in the RDS was proposed [37,38].

Here, the focus is on nanocatalysts that have attracted most of the attention during the last two decades, for which the NP support has played an essential role [39–49]. In

particular, porous materials including metal–organic frameworks (MOFs) have been a privileged type of NP support, because the NP catalyst can be formed and encapsulated inside MOFs for efficient nanocatalysis [50–57]. Therefore, hydrophilic late transition-metal salts are introduced in water, for instance, into the cavity of the zeolitic imidazolate framework (ZIF) [58], for which ZIF-8 [59–61] has been very successful in our laboratory using reduction with $NaBH_4$ [62] of the transition-metal cation to NP inside the ZIF-8 cavity [18,63–67] (Scheme 1).

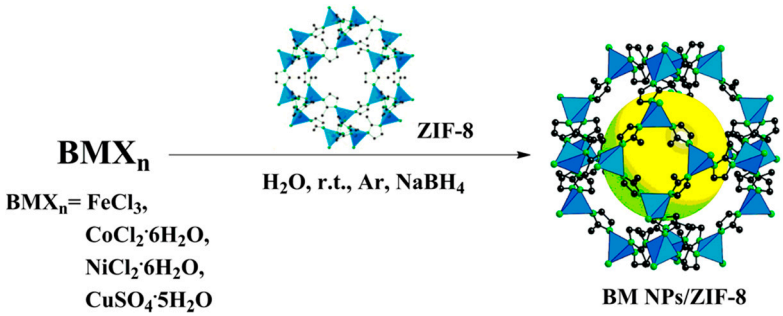

Scheme 1. Reproduced with permission from Ref. [63]. Copyright 2017 American Chemical Society.

Under these conditions, Ni was shown to be the most catalytically effective first-row transition metal with an Ni NP size of 2.7 nm inside ZIF-8. In the presence of 0.3 N that appears to favor the catalysis, the turnover frequency (TOF) at 25 °C was of 85.7 $mol_{H2} \cdot mol_{cat.}{}^{-1} \cdot min^{-1}$ [63]. The reaction is first-order in catalyst concentration and zero-order in AB concentration, an indication that the role of AB in the transition state is not significant. This is confirmed by a kinetic isotope effect (KIE) with D_2O ($KIE = k_{H2O}/k_{D2O}$) of 2.49, suggesting that water O-H bond cleavage is the rate-determining step (RDS). The favorable influence of OH^- on the reaction rate was taken into account by OH^- coordination onto the Ni NP surface, increasing the electron density on Ni, which is favorable for water O-H oxidative addition onto surface Ni atoms. Meanwhile, on–off control of the H_2 evolution was demonstrated upon successive addition of OH^- that activated H_2 evolution and H^+ that stopped the reaction (Figure 3) [63].

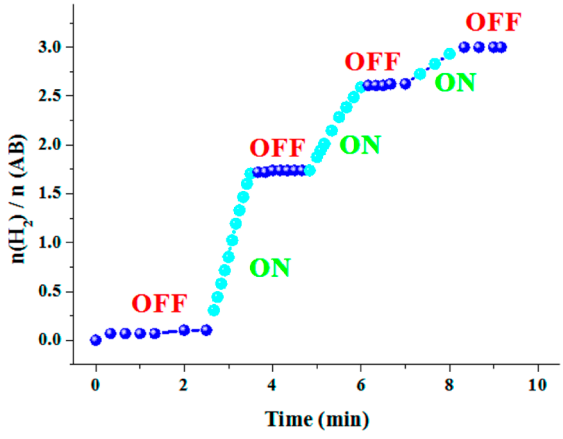

Figure 3. On–off control of H_2 evolution during Ni NP@ZIF-8-catalyzed AB hydrolysis upon successive addition of NaOH (on) and HCl (off) in water. Reproduced with permission from Ref. [63]. Copyright 2017 American Chemical Society.

3.3. Use of a Transition-Metal-Alloyed Catalyst

Heterobimetallic catalysts often result in positive synergistic effects [68,69], and Hou et al. synthesized graphene-oxide-supported bimetallic Ni-Co catalysts reaching a TOF of 154 $mol_{H2} \cdot mol_{cat.}{}^{-1} \cdot min^{-1}$ at ambient temperature [68]. A remarkable result was obtained

in our group with Pt-Ni NPs in ZIF-8 (Ni_2Pt@ZIF-8) for which the TOF value reached 669.3 $mol_{H2} \cdot mol_{cat.}^{-1} \cdot min^{-1}$. The synthesis of NiPt NP@ZIF-8 is shown in Scheme 2 [64].

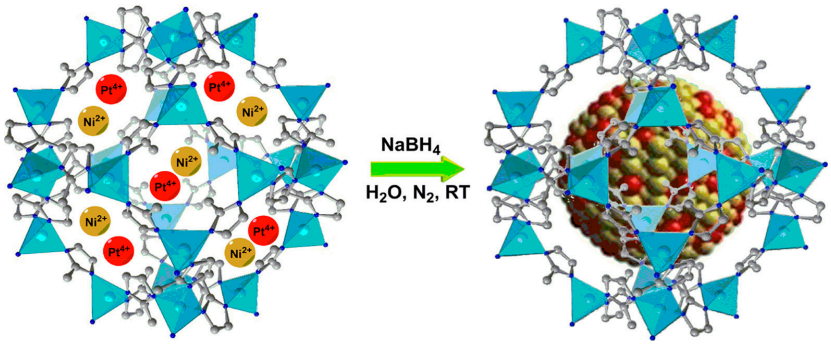

Scheme 2. Reproduced with permission from Ref. [63]. Copyright 2017 American Chemical Society.

This high TOF value was 87 times higher than the TOF of Pt@ZIF-8 under similar conditions, as a result of a positive volcano-type type synergy between Ni and Pt. The suggested mechanism was related to that with Ni@ZIF-8, and the primary KIE with D_2O was high (4.67), showing that water O-H cleavage was the RDS [63]. A considerable volcano-type positive synergy in catalytic efficiency was also obtained with Co-Pt NPs embedded in "click" dendrimers. In these "click" dendrimers that contain crucial triazole ligands, the nanocatalysts were encapsulated inside the dendrimer by coordination onto these ligand groups bridging the dendrimer core to the dendrimer periphery (Figure 4). In the presence of 0.3 M NaOH, the TOF value was 476.2 $mol_{H2} \cdot mol_{catal}^{-1} \cdot min^{-1}$ (952.4 $mol_{H2} \cdot mol_{Pt}^{-1} \cdot min^{-1}$). In both the ZIF-8 (endoreceptor) and click dendrimers (exoreceptors), the N atoms of the support played an important role in the confinement of the catalyst together with the substrates, and similar mechanistic trends were observed with both supports (Scheme 3) [70].

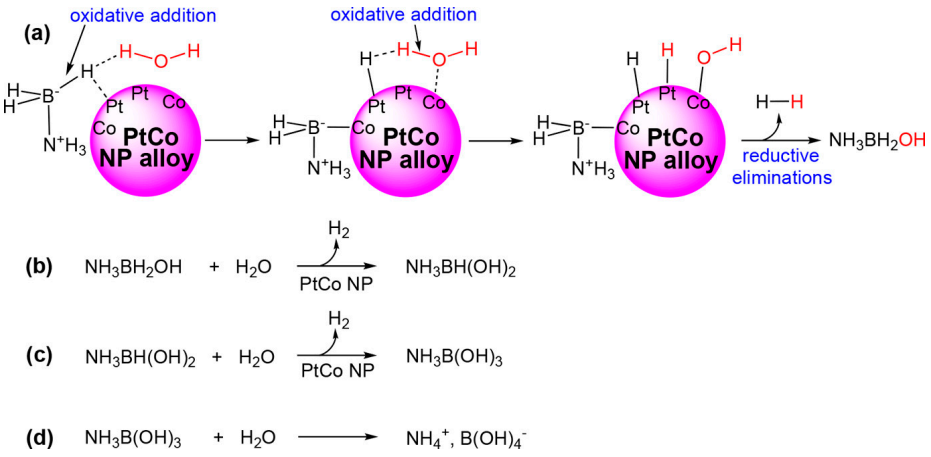

Scheme 3. Proposed mechanism for AB hydrolysis catalyzed by PtCo alloy@"click" dendrimer. A similar mechanism was suggested for catalysis by PtNi alloy@ZIF-8. In both cases, the N atom coordination of the support framework to the alloy surface increases the intermetallic synergy in the alloy and synergy with the framework. (**a**–**c**) successively represent the formation of the first, second and third mol hydrogen, and (**d**) shows the formation of the final salt. Reproduced with permission from Ref. [70]. Copyright 2019 American Chemical Society.

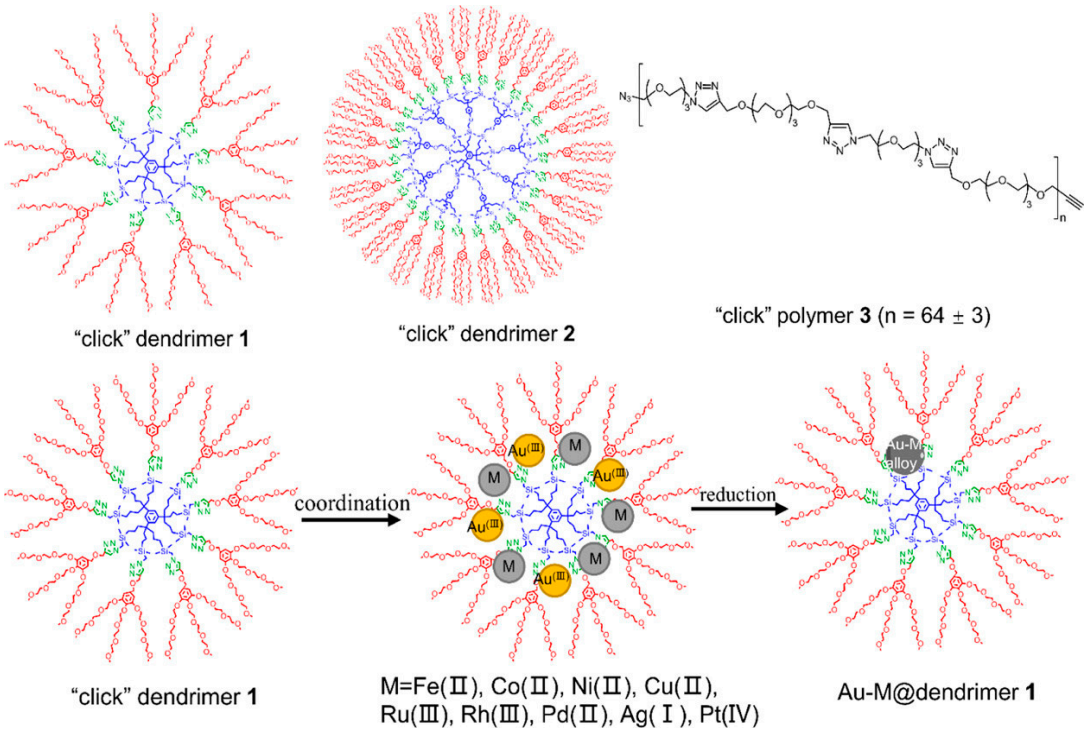

Figure 4. "Click" dendrimers (i.e., dendrimer assembled by click chemistry, vide supra) and a "click" polymer reference allowing the investigation of the dendrimer effect in NP stabilization and efficiency (**top**). The green-colored cycles in all the dendrimers represent 1,2,3-triazoles formed upon Cu-alkyne-azide catalysis (CuAAC) by the "click" reaction between polyazido-terminated dendrimer cores and dendrons containing a terminal alkyne at their focal point. The incorporation of triazole-coordinated metal ions inside the "click" dendrimer followed by reduction using $NaBH_4$ to dendrimer-encapsulated NPs (**bottom**). Reproduced with permission from Ref. [70]. Copyright 2020 American Chemical Society.

Plasmon excitation by visible light is useful in nanocatalysis [71–80], including for H_2 evolution from AB [76–78]. When the bimetallic nanocatalyst included Au as one of the two metals, excitation of the Au plasmon by illumination with visible light boosted H_2 evolution, with the most efficient light effects being observed upon combining Au with M = Co, Ni, Ru, Rh, or Pt. The evolution of 3 mol H_2 was observed in down to 1.3 min at 25 °C, 3 times faster than in the dark. Co was found to be the best first-raw transition metal alloyed with Au [78]. This boosting effect was taken into account by the plasmon-induced "hot" electron transfer, from Au to the other late transition metal M in the alloy, enriching the electron density on M, which enhances activation of the substrates [78,79]. Indeed, in the reaction mechanism, it is the transition metal atom M at the surface that is responsible for water O-H bond cleavage by oxidative addition of this bond in the rate-determining step (RDS). The increase in electron density at this metal center, such as the one provided from the plasmonic metal by "hot" electron transfer, largely favors this oxidative addition (vide infra). Primary KIEs observed using D_2O under dark conditions and found to be even larger under visible-light irradiation confirmed that O-H bond cleavage was largely involved in the RDS. In the initial hydride transfer from AB to the nanocatalyst, it appears that water is not significantly involved (contrary to $NaBH_4$ as the H_2 source, because the negatively charged BH_4^- anion is more significantly hydrogen-bonded to water than in neutral AB). On the other hand, after such a hydride transfer (or oxidative addition of the B-H bond immediately followed by B to NP electron transfer), the nanocatalyst becomes negatively charged, which increases the ability of water activation by oxidative addition onto the active late transition metal M (but not Au alone, which is a very poor nanocatalyst of the reaction). The increase in electron density at the active metal site is still considerably

enhanced by the plasmonic hot electron transfer. Thus, the anionic $[NP\text{-}H]^-$ intermediate is likely to form a hydrogen bond with water, $[NP\text{-}H]^-$–H–OH, removing some electron density from the water O–H bond, which further facilitates oxidative addition of this bond onto the activated transition-metal surface. This first reaction phase ends by reductive elimination of the two hydride ligands forming H_2 and the OH and NH_3BH_2 ligands providing NH_3BH_2OH that, in turn, undergoes H_2 formation according to a similar process (Scheme 1) [78].

4. Catalyzed H_2 Generation upon AB Methanolysis

It is striking that AB methanolysis (Equation (6)) has been so much less studied than AB hydrolysis.

$$NH_3BH_3 + 4CH_3OH \xrightarrow{\text{catalyst}} NH_4B(OCH_3)_4 + 3H_2 \quad (6)$$

The seminal AB methanolysis publication is that of Ramachandran and Gagare who reported in 2007 both optimized ammonia borane preparation and its methanolysis [33]. These authors utilized, for AB methanolysis, late transition-metal catalysts, both of the first-row metals and noble metals ($CoCl_2$, Raney Ni, Pd/C, $RuCl_3$ and $RhCl_3$), with $RuCl_3$ being found as the best catalyst. With this catalyst, they obtained a TOF value of 150 $mol_{H2}{\cdot}mol_{catal}{}^{-1}{\cdot}min^{-1}$, which already was a very good performance compared to all those obtained afterward (vide infra) and up to now. Jagirdar's group reported Co, Ni, and Cu-based nanocatalysts (including oxides and bimetallic Ni-Cu alloys), avoiding the use of noble metals [81,82]. Among all the AB methanolysis reports up to now (most of the reported TOF values are below 100 $mol_{H2}{\cdot}mol_{catal}{}^{-1}{\cdot}min^{-1}$), a remarkable performance in terms of TOF value for this reaction was obtained by Sun's group with 366.4 $mol_{H2}{\cdot}mol_{catal}{}^{-1}{\cdot}min^{-1}$ using a Ag-Pd nanocatalyst, $Ag_{30}Pd_{70}$, synthesized by the coreduction of $AgNO_3$ and $PdCl_2$ in the presence of oleylamine, supported on carbon [83]. Another very efficient catalyst reported by Lu's group contained ultrafine Rh NPs (1.4–2.6 nm) confined in a covalent organic framework (COF) synthesized from piperazine and cyanuric chloride, and it produced a TOF of 505 $mol_{H2}{\cdot}mol_{catal}{}^{-1}{\cdot}min^{-1}$ at 298 K. Given the temperature effect decreasing the TOF value upon decreasing the temperature, such high TOF values ensure applicability for low-temperature devices [84].

The same group recently reported an even better catalyst, a porphyrin-derived N-doped porous carbon-confined Ru NP for AB methanolysis with a very high TOF value of 727 $mol_{H2}{\cdot}mol_{catal}{}^{-1}{\cdot}min^{-1}$ at 25 °C [85]. Luo et al. reported L-proline (PRO)-capped Rh NPs as a catalyst with an AB methanolysis TOF of 1035 $mol_{H2}{\cdot}mol_{catal}{}^{-1}{\cdot}min^{-1}$ and 0.3 M NaOH that is known to boost late transition-metal nanocatalysts of AB solvolysis (vide supra). The presence of a suitable O- and N-rich PRO template also contributes to the positive synergy. At 0 °C, this nanocatalyst was still effective in ethanol that is less toxic than methanol, with these trends being useful toward low-temperature portable applications [86]. The best AB methanolysis performance so far was obtained by Zahmakiran's group using nanocatalyst MIL-101-decorated Pd NPs with TOF = 1080 $mol_{H2}{\cdot}mol_{catal}{}^{-1}{\cdot}min^{-1}$ at room temperature [87].

The literature on AB methanolysis has recently been reviewed by Xu's group [8], Li and Wang's group [88], and Özkar [89], and reports on nanocatalysts have appeared based on first-row late transition-metals [8,90], and also on noble metals [90–92].

H_2 evolution upon AB methanolysis presents several advantages over the method using AB hydrolysis toward applications [8,88,91]: (i) AB is highly soluble in methanol under ambient conditions (23 wt%) [33,92]; (ii) AB is very stable in methanol in the absence of a catalyst; (iii) H_2 evolution upon methanolysis of AB is pure without ammonia (contrary to AB hydrolysis), which is an impurity poisoning fuel cells; (iv) AB methanolysis produces H_2 at low temperature if the nanocatalyst is efficient enough (methanol freezes at (−97.8 °C), which could be useful toward portable devices at cold temperatures); (v) $NH_4B(OCH_3)_4$ that is formed upon AB methanolysis readily reacts with $LiAlH_4$ and NH_4Cl at room

temperature to regenerate AB, whereas the regeneration of $NH_4B(OH)_4$ formed upon AB hydrolysis is more complicated [33,89].

AB methanolysis is, in general, as for AB hydrolysis, first-order in catalyst concentration and zero-order in AB concentration, and the mechanism has been suggested to involve O-H cleavage in the RDS [81–93]. For instance, along this line, Lu's group, in their work noted above on porphyrin-derived N-doped porous carbon-confined Ru NPs, indicated that AB methanolysis of both NH_3BD_3 and $^{15}NH_3BH_3$ in CH_3OH showed secondary KIEs of 1.29 and 1.05, respectively, and methanolysis of NH_3BH_3 in CD_3OD involved a primary KIE of 5.78. These results clearly showed the key role of methanol in the RDS step of AB methanolysis [85].

AB methanolysis was also recently catalyzed by Au-Pd@ ZIF-8, generated by reducing equimolar amounts of $HAuCl_4$ and Na_2PdCl_4 by $NaBH_4$ in methanol in the presence of ZIF-8, with the reaction being 3.7 times faster under visible-light illumination than in the dark. KIE values measured in CD_3OD were 2.2 and 3.4, respectively, in agreement with O–H bond cleavage as the RDS. Synergy effects between Pd and Au were taken into account in DFT calculations by the d-orbital density of states (DOS) of different NPs, with the d-band center of Au (111) and Pd (111) being −3.2 and −2.4 eV, respectively, whereas, upon alloying, the d-band center of AuPd (111) was −1.5 eV, at a higher energy than those of both Au (111) and Pd (111). Thus, the d orbital of the metal in AuPd is closer to the energy level of the antibonding orbital of the adsorbate species than with the related Au and Pd nanocatalysts, signifying a higher AB adsorption energy on AuPd. Upon illumination, a hot plasmon Au electron is injected into the Pd-AB adsorbate, increasing the electron density on Pd toward the methanol O–H oxidative addition onto the Pd surface center of the alloy, as confirmed by the DFT calculations (Scheme 4) [93].

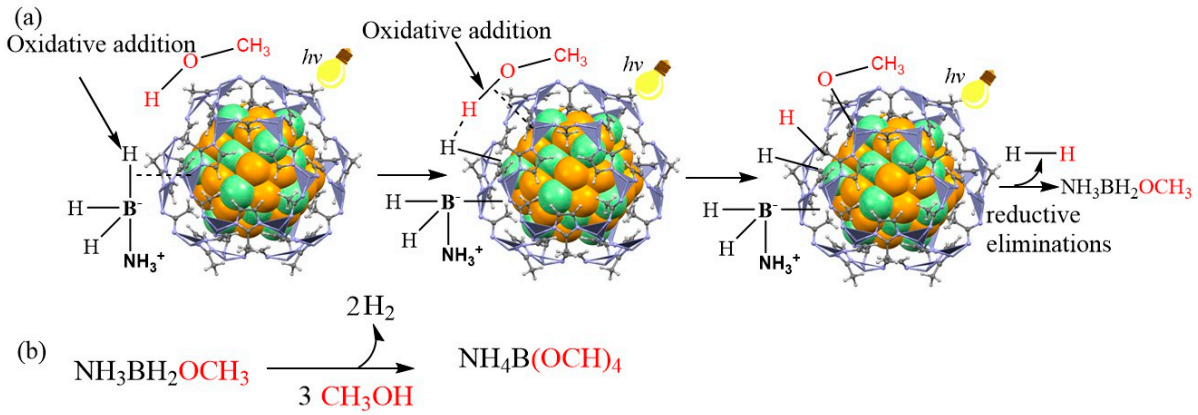

Scheme 4. Mechanism of AuPd@ZIF-8 catalysis of AB methanolysis in the dark and under visible-light irradiation. The initial step involves hydride transfer from AB to the catalyst surface (or oxidative addition of the B-H bond followed by electron transfer from B^- to the NP), then H bonding $[NP\text{-}H]^-$–H–OCH_3 between the nucleophilic negatively charged $[NP\text{-}H]^-$ species and the electrophilic methanol proton (attracting CH_3OH near the NP surface). This decreases the CH_3O–H bond electron density, facilitating further oxidative addition of this O–H bond onto Pd, which is boosted by the plasmonic hot electron transfer under visible illumination. (**a**) Mechanistic aspects of the formation of the first mol H_2. (**b**) formation of the second and and third mol H_2. Reproduced with permission from Ref. [93]. Copyright 2023 Royal Society of Chemistry.

Alternatively, Yamashita's group examined photocatalytic H_2 generation over the Au/TiO_2 nanocatalyst from AB decomposition. This reaction was shown to be initiated by the generation of plasmon-induced charge pairs. It is not known, however, how the RDS would change upon AB methanolysis compared to hydrolysis in this process [94].

5. Comparison between AB Hydrolysis and Methanolysis

AB solvolysis is a superb and the most studied efficient method of H_2 generation, because AB is safe, stable in water and methanol under ambient conditions, and can now be obtained in >99% purity. Both AB hydrolysis and methanolysis produce 3 mol H_2 per mol AB, but the H_2 produced by hydrolysis contains all the more NH_3 as the AB concentration is higher, which is damaging, because NH_3 is poisoning fuel cells, whereas the H_2 produced by AB methanolysis is pure from NH_3 impurities. This is a very important advantage of methanolysis over hydrolysis, although nanocatalyzed AB hydrolysis proceeds faster than methanolysis. Another important parameter is the temperature, because hydrolysis is limited to reactions above 0 °C, the freezing point of water, whereas AB methanolysis can be operated at low to very low temperatures that are not limited by the extremely low freezing point of methanol as long as the catalyst is reactive enough at these low temperatures. Another essential parameter is the regeneration of AB from the AB solvolysis side product, $NH_4B(OH)_4$ in the case of hydrolysis, and $NH_4B(OCH_3)_4$ in the case of AB methanolysis. This AB regeneration is much more complicated in the case of hydrolysis than in that of methanolysis, because $NH_4B(OCH_3)_4$ is easily converted to AB upon reaction with $LiAlH_4$ and NH_4Cl, as reported by Ramachandran [33], whereas $NH_4B(OH)_4$ must first be converted to $NH_4B(OCH_3)_4$ by reaction with methanol (Equation (7), Scheme 5). However, the recycling of $LiAl(OMe)_4$ has not yet been conducted (Scheme 5) [33,88]

$$NH_4B(OCH_3)_4 + NH_4Cl + LiAlH_4 \rightarrow \underset{\substack{81\%\ \text{yield}\\ >98\%\ \text{purity}}}{NH_3BH_3} + Al(OCH_3)_3 + CH_3OH + H_2 + LiCl + NH_3 \quad (7)$$

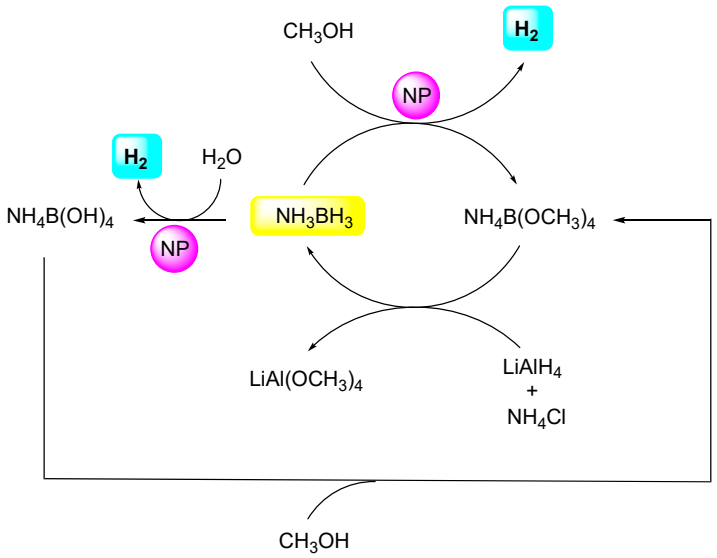

Scheme 5. AB hydrolysis and methanolysis and AB regeneration after solvolysis. The regeneration of AB from AB methanolysis needs a reaction with $LiAlH_4$ and NH_4Cl of the AB methanolysis product, $NH_4B(OCH_3)_4$, in THF (0 °C to r.t., 90% yield), but the regeneration of the AB hydrolysis product $NH_4B(OH)_4$ is more complicated, because it first requires a reaction with methanol. $LiAl(OMe)_4$ can be prepared by the disproportionation of $LiAl(OMe)_3H$ and is insoluble [95]. Inspired by Refs. [32,87]. Copyright 2007 and 2022. American Chemical Society.

The energy-consuming step in AB regeneration is the reduction of the strong bonds B-O in $B(OCH_3)_3$ or $NH_4B(OH)_4$, produced by AB solvolysis, which must proceed using a hydride such as $LiAlH_4$ Equation (7) [92].

A comparison of the mechanisms of nanocatalyzed AB dehydrogenative hydrolysis and methanolysis suggests that methanolysis is more boosted (3.7 times) by visible-light illumination compared to the reaction in the dark than hydrolysis (1.4 time). The KIE increased from 2.2 in the dark to 3.4 under illumination for AB methanolysis, but only from

4 to 4.3 for AB hydrolysis. This shows that visible light has much more influence on AB methanolysis than on AB hydrolysis. Upon examining the hydrogen bonding between the anionic hydridic species $[Pd–H]^-$, formed by hydride transfer from AB to the NP, and the acidic solvent O–H bond, this bond is stronger upon AB hydrolysis than upon AB methanolysis, as water is more acidic than methanol. Consequently, solvent O–H bond weakening is more significant with water than with methanol, and solvent O–H bond oxidative addition on the nanocatalyst surface is easier with water than with methanol. This explains that the additional activation by visible light is necessary upon AB methanolysis compared to AB hydrolysis [66,78,93].

6. Conclusions

Among the H-rich H_2 sources [1], AB stands as one of the best suppliers upon solvolysis, either hydrolysis or alcoholysis. This issue has been raised by the seminal report from Chandra and Xu in 2006 on AB hydrolysis [4]. Since then, considerable efforts have been devoted to improvements toward safe and efficient H_2 production upon AB solvolysis. In particular, interest in these H_2 generation methods has been boosted by the in-depth seminal work by the Ramachandran group, since 2007, who disclosed that the AB methanolysis reaction improved AB synthesis and proposed its regeneration from AB solvolysis reactions [28,30,33].

Given the AB stability in water and alcohols, catalysis, particularly nanocatalysis by late transition-metal NPs and alloys stabilized by optimized supports, plays the central role in H_2 production from AB solvolysis. As in most catalytic reactions, noble metals (Ru, Rh, Pd, and Pt), despite their toxicity, high price, and scarcity, are more efficient than non-noble metals, i.e., those of the first-row transition metals (Co, Ni, Cu), but synergies among these metals and with the support can increase catalytic efficiencies, particularly doping with other elements such as B or P. Studies involving single-atom catalysts are also awaited [95,96]. Nanoporous supports are especially efficient and useful [97], because they favor the formation of ultrasmall and thus very efficient nanocatalysts and protects them from aggregation.

In comparing AB hydrolysis and methanolysis, it quickly appeared that AB hydrolysis encountered a major problem in that the AB hydrolysis product was all the more contaminated by NH_3 as the AB concentration was higher, which was damaging due to the NH_3 poisoning of fuel cells [98,99]. On the other hand, the H_2 produced is pure upon methanolysis.

The other drawback of AB hydrolysis is the regeneration after hydrolysis that is longer and more complex than regeneration after AB methanolysis. Finally, the last drawback is that the temperature window is much more limited for hydrolysis, due to water freezing at 0 °C, compared to methanolysis.

Favorable points for hydrolysis in comparison with methanolysis are that water is cheaper and less toxic than methanol and that the hydrolysis reactions are faster than the methanolysis reactions. Yet, TOFs of the AB methanolysis reaction with sophisticated nanocatalysts have very recently approached or overtaken 1000 $mol_{H2}{\cdot}mol_{cat.}{}^{-1}{\cdot}min^{-1}$, allowing perspectives for the application to low-temperature devices [84–86]. Ethanol is less toxic than methanol, but nanocatalyzed reactions are slower in ethanol than in methanol.

In summary, the most critical issue for AB solvolysis is the high cost of AB and of its regeneration after solvolysis, even more so for hydrolysis than for methanolysis. More research is required for improvements in catalysts and supports, particularly with emphasis on non-noble metal nanocatalysts. Up-to-date investigation tools such as in situ XRD, electron microscopies, X-ray absorption, theoretical calculations, and Machine Learning [100] should help the improvements, scaling, and transfer to industry for device applications toward an "H_2 economy".

Author Contributions: Conceptualization, N.K., C.W. and D.A.; methodology, N.K., C.W. and D.A.; software, N.K., C.W. and D.A.; validation, C.W. and D.A.; formal analysis, N.K., C.W. and D.A.; investigation, N.K., C.W. and D.A.; resources, C.W. and D.A.; data curation, N.K., C.W. and D.A.; writing—original draft preparation, NK.; writing—review and editing, C.W. and D.A.; visualization, N.K., C.W. and D.A.; supervision, C.W. and D.A.; project administration, D.A.; funding acquisition, D.A. All authors have read and agreed to the published version of the manuscript.

Funding: Financial support from the Chinese Scholarship Council (CSC grant to N.K.), the National Natural Science Foundation of China (No. 21805166), the start-up funding by Beijing University of Technology (C.W.), the University of Bordeaux, and the Centre National de la Recherche Scientifique (CNRS) is gratefully acknowledged.

Data Availability Statement: Not applicable.

Acknowledgments: Outstanding contributions and fruitful discussions concerning original works with colleagues and former students cited in references, in particular, Fangyu Fu and Wang Qi in the University of Bordeaux, are gratefully acknowledged.

Conflicts of Interest: The authors declare no conflict of interest.

References

1. He, T.; Pachfule, P.; Wu, H.; Xu, Q.; Chen, P. Hydrogen Carriers. *Nat. Rev. Mater.* **2016**, *1*, 16059. [CrossRef]
2. Lebrouhi, B.E.; Djoupo, J.J.; Lamrani, B.; Benabdelaziz, K.; Kousksou, T. Global Hydrogen Development—A Technical and Geopolitical Overview. *Int. J. Hydrogen Energy* **2022**, *47*, 7016–7048. [CrossRef]
3. Zhu, J.; Hu, L.; Zhao, P.; Lee, L.Y.S.; Wong, K.Y. Recent Advances in Electrocatalyic Hydrogen Evolution. *Chem. Rev.* **2020**, *120*, 851–918. [CrossRef] [PubMed]
4. Chandra, M.; Xu, Q.J. A High-Performance Hydrogen Generation System: Transition Metal-Catalyzed Dissociation and Hdrolysis of Ammonia-Borane. *Power Sources* **2006**, *156*, 190–194. [CrossRef]
5. Hamilton, C.W.; Baker, R.T.; Staubitz, A.; Manners, I. B–N compounds for chemical hydrogenstorage. *Chem. Soc. Rev.* **2009**, *38*, 279–293. [CrossRef]
6. Staubitz, A.; Robertson, A.P.M.; Manners, I. B-N Compounds for Chemical Hydrogen Storage. *Chem. Rev.* **2010**, *110*, 4079–4124. [CrossRef]
7. Wang, P. Molecular Systems for Ligh-Driven Hydrogen Production. *Dalton Trans.* **2012**, *41*, 4296e302.
8. Zhan, W.-W.; Zhu, Q.-L.; Xu, Q. Dehydrogenation of Ammonia Borane by Metal Nanoparticle Catalysts. *ACS Catal.* **2016**, *6*, 6892–6905. [CrossRef]
9. Li, Z.; Xu, Q. Metal-Nanocatalyzed Hydrogen Generation from Formic Acid. *Acc. Chem. Res.* **2017**, *50*, 1449–1458. [CrossRef]
10. Yu, X.; Tang, Z.; Sun, D.; Ouyang, L.; Zhu, M. Recent Advances and Remaining Challenges of Nanosctuctured Materials for Hydrogen Storage Applications. *Prog. Mater. Sci.* **2017**, *88*, 1–48. [CrossRef]
11. Demici, U.B. Ammonia borane, a material with exceptional properties for ammonia borane storage. *Int. J. Hydrogen Energy* **2017**, *42*, 9978–10013. [CrossRef]
12. Zhu, B.; Zou, R.; Xu, Q. Metal-Organic Framework Based Catalysts for Hydrogen Evolution. *Adv. Energy Mater.* **2018**, *8*, 1801193. [CrossRef]
13. Akbayrak, S.; Özkar, S. Ammonia borane as hydrogen storage materials. *Int. J. Hydrogen Energy* **2018**, *43*, 18592–18606. [CrossRef]
14. Sun, Q.M.; Wang, N.; Xu, Q.; Yu, J. Nanopore-Supported Metal Nanocatalysts for Efficient Hydrogen Generation from Liquid Phase Chemical Hydrogen Storage. *Adv. Mater.* **2020**, *32*, 2001818. [CrossRef] [PubMed]
15. Huang, Z.G.; Wang, S.N.; Dewhurst, R.D.; Ignat'ev, N.V.; Finze, M.; Braunschweig, H. Boron: Its Role in Energy-Related Processes and Applications. *Angew. Chem. Int. Ed.* **2020**, *59*, 8800–8816. [CrossRef] [PubMed]
16. Axet, M.R.; Philippot, K. Catalysis with Colloidal Ruthenium Nanoparticles. *Chem. Rev.* **2020**, *120*, 1085–1145. [CrossRef] [PubMed]
17. Yao, Q.L.; Ding, Y.; Lu, Z.-H. Nobel-metal free catalysts for hydrogen generation from boron- and nitrogen-based hydrides. *Inorg. Chem. Front.* **2020**, *7*, 3837–3874. [CrossRef]
18. Wang, C.; Wang, Q.; Fu, F.; Astruc, D. Hydrogen Generation from Nanocatalyzed Hydrolysis of Hydrogen-Rich Boron Derivatives: Recent Developments. *Acc. Chem. Res.* **2020**, *53*, 2483–2493. [CrossRef]
19. Wang, C.; Astruc, D. Recent Developments of Liquid-Phase Hydrogen Generation. *Chem. Soc. Rev.* **2021**, *50*, 3437–3484. [CrossRef]
20. Yue, M.; Lambert, H.; Pahon, E.; Roche, R.; Jemei, S.; Hissel, D. Hydrogen Energy Systems: A Critical Review of Technologies, Applications, Trends and Challenges. *Renew. Sustain. Energy Rev.* **2021**, *146*, 111180. [CrossRef]
21. Lau, S.; Gasperini, D.; Webster, R.L. Ammonia Boranes as Transfer Hydrogenation and Hydrogenation Reagents. *Angew. Chem. Int. Ed.* **2021**, *6*, 14272–14294. [CrossRef] [PubMed]
22. Mboyi, C.D.; Poinsot, D.; Roger, J.; Fajerwerg, K.; Kahn, M.L.; Hierso, J.-C. The Hydrogen-Storage Challenge: Nanoparticles for Metal-Catalyzed Ammonia Borane Dehydrgenation. *Small* **2021**, *17*, 2102759. [CrossRef] [PubMed]

23. Liu, X.; Zhang, X.; Li, D.-S.; Zhang, S.; Zhang, Q.J. Recent Advances in the "On-Off" Approaches for the on-Demand Liquid-Phase Hydrogen Evolution. *Mater. Chem. A* **2021**, *9*, 18164–18174. [CrossRef]
24. Klooster, W.T.; Koetzle, T.F.; Siegbahn, P.E.M.; Richardson, T.B.; Crabtree, R.H. Study of the NH···H-B Dihydrogen Bond Including the Crystal Structure of BH_3NH_3 by Neutron Diffraction. *J. Am. Chem. Soc.* **1999**, *121*, 6337–6343. [CrossRef]
25. Plumley, J.A.; Evanseck, J.D. Covalent and Ionic Nature of the Dative Bond and Account of Accurate Ammonia-Borane Binding Enthalpies. *J. Phys. Chem. A* **2007**, *111*, 13472–13483. [CrossRef]
26. Shore, S.G.; Parry, R.W. The Cystalline Compound Ammonia Borane, H_3NBH_3. *J. Am. Chem. Soc.* **1955**, *77*, 6084–6085. [CrossRef]
27. Li, H.; Yang, Q.; Shore, S.G. Ammonia Borane, Past as Prolog. *J. Organomet. Chem.* **2014**, *751*, 60–66. [CrossRef]
28. Ramachandran, P.V.; Raju, B.C.; Gagare, P.D. One-Pot Synthesis of Ammonia-Borane and Trialkylamine-Borane from Trimethyl Borate. *Org. Lett.* **2012**, *14*, 6119–6121. [CrossRef]
29. Schlesinger, H.I.; Brown, H.C.; Mayfield, D.L.; Gilbreath, J.R. The Preparation of Other Borohydrides by Metathetical Reactions Utilizing the Metal Alkali Borohydrides. *J. Am. Chem. Soc.* **1953**, *75*, 213–215. [CrossRef]
30. Ramachandran, P.V.; Kulkarni, A.S. Open Flask Synthesis of Amine Boranes via Tandem Amine-Ammonium Salt Equilibration-Metathesis. *Inorg. Chem.* **2015**, *54*, 5618–5620. [CrossRef]
31. Wiedner, E.S.; Chambers, M.B.; Pitman, C.L.; Bullock, R.M.; Miller, A.J.M.; Appel, A.M. Thermodynamic Hydricity of Transition Metal Hydrides. *Chem. Rev.* **2016**, *116*, 8655–8692. [CrossRef] [PubMed]
32. Chandra, M.; Xu, Q.J. Dissociation and hydrolysis of ammonia-borane with solid acids and carbon dioxide: An efficient hydrogen generation system. *Power Sources* **2006**, *159*, 855–860. [CrossRef]
33. Ramachandran, P.V.; Gagare, P.D. Preparation of Ammonia Borane in High Yield and Purity, Methanolysis, and Regeneration. *Inorg. Chem.* **2007**, *46*, 7810–7817. [CrossRef] [PubMed]
34. Bhattacharya, P.; Krause, J.A.; Guan, H. Mechanistic Studies of Ammonia Borane Dehydrogenation Catalyzed by Iron Pincer Complexes. J. *Am. Chem. Soc.* **2014**, *136*, 11153–11161. [CrossRef] [PubMed]
35. Astruc, D. Transition-metal radicals: Chameleon structure and catalytic function. *Acc. Chem. Res.* **1991**, *24*, 36–42. [CrossRef]
36. Buss, J.A.; Edouard, G.A.; Cheng, C.; Shi, J.; Agapie, T. Molybdenum Catalyzed Ammonia Borane Dehydrogenation. *J. Am. Chem. Soc.* **2014**, *136*, 11272–11275. [CrossRef]
37. Chen, W.; Li, D.; Wang, Z.; Qian, G.; Sui, Z.; Duan, X.; Zhou, X.; Yeboah, I.; Chen, D. Reaction mechanism and kinetics for hydrolytic dehydrogenation of ammonia borane on a Pt/CNT catalyst. *AIChE J.* **2017**, *63*, 60–65. [CrossRef]
38. Li, Z.; He, T.; Liu, L.; Chen, W.; Zhang, M.; Wu, G.; Chen, P. Covalent triazine framework supported non-noble metal nanoparticles with superior activity for catalytic hydrolysis of ammonia borane: From mechanistic study to catalyst design. *Chem. Sci.* **2017**, *8*, 781–788. [CrossRef]
39. Corma, A.; Garcia, H. Supported gold nanoparticles as catalysts for organic reactions. *Chem. Soc. Rev.* **2008**, *37*, 2096–2126. [CrossRef]
40. Statakis, M.; Garcia, H. Catalysis by Supported Gold Nanoparticles: Beyond Aerobic Oxidative Processes. *Chem. Rev.* **2012**, *112*, 4469–4506. [CrossRef]
41. Polshettiwar, V.; Cha, D.; Zhang, X.X.; Basset, J.M. High-Surface-Area Silica Nanospheres (KCC-1) with a Fibrous Morphology. *Angew. Chem. Int. Ed.* **2010**, *49*, 9652–9656. [CrossRef] [PubMed]
42. Figri, A.; Bouhrara, M.; Nekoueishahraki, B.; Basset, J.M.; Polshettiwar, V. Nanocatalysts for Suzuki cross-coupling reactions. *Chem. Soc. Rev.* **2011**, *40*, 5181–5203.
43. Narayanan, R.; El-Sayed, B.J. Catalysis with Transition Metal Nanoparticles in Colloidal Solution: Nanoparticle Shape Dependence and Stability. *Phys. Chem. B* **2005**, *109*, 12663–12676. [CrossRef] [PubMed]
44. Shifrina, Z.B.; Matveeva, V.G.; Bronstein, M. Role of Polymer Structures in Catalysis by Transition Metal and Metal Oxide Nanoparticle Composites. *Chem. Rev.* **2020**, *120*, 1350–1396. [CrossRef]
45. Li, G.; Jin, R.C. Atomically Precise Gold Nanoclusters as New Model Catalysts. *Acc. Chem. Res.* **2013**, *46*, 1749–1758. [CrossRef]
46. Niu, Z.Q.; Li, Y.D. Removal and Utilization of Capping Agents in Nanocatalysis. *Chem. Mater.* **2014**, *26*, 72–83. [CrossRef]
47. Gawande, M.B.; Shelke, S.N.; Sboril, R.; Varma, R.S. Microwave-Assisted Chemistry: Synthetic Applications for Rapid Assembly of Nanomaterials and Organics. *Acc. Chem. Res.* **2014**, *47*, 1338–1348. [CrossRef]
48. Astruc, D.; Heuze, K.; Gatard, S.; Méry, D.; Nlate, S.; Plault, L. Metallodendritic Catalysis for Redox and Carbon—Carbon Bond Formation Reactions: A Step towards Green Chemistry. *Adv. Syn. Catal.* **2005**, *347*, 329–338. [CrossRef]
49. Astruc, D. Introduction: Nanoparticles in Catalysis. *Chem. Rev.* **2020**, *120*, 461–463. [CrossRef] [PubMed]
50. Corma, A.; Garcia, H.; Xamena, F.X.L. Engineering Metal Organic Frameworks for Heterogeneous Catalysis. *Chem. Rev.* **2010**, *110*, 4606–4655. [CrossRef]
51. Viciano-Chumillas, M.; Mon, M.; Ferrando-Soria, J.; Corma, A.; Leyva-Perez, A.; Armentano, D.; Pardo, E. Metal–Organic Frameworks as Chemical Nanoreactors: Synthesis and Stabilization of Catalytically Active Metal Species in Confined Spaces. *Acc. Chem. Res.* **2020**, *53*, 520–531. [CrossRef] [PubMed]
52. Choi, K.M.; Na, K.; Somorjai, G.A.; Yaghi, O.M. Chemical Environment Control and Enhanced Catalytic Performance of Platinum Nanoparticles Embedded in Nanocrystalline Metal–Organic Frameworks. *J. Am. Chem. Soc.* **2015**, *137*, 7810–7816. [CrossRef] [PubMed]
53. Dhakshinamoorthy, A.; Li, Z.H.; Garcia, H. Catalysis and photocatalysis by metal organic frameworks. *Chem. Soc. Rev.* **2018**, *47*, 8134–8172. [CrossRef] [PubMed]

54. Dhakshinamoorthy, A.; Asiri, M.; Garcia, H. Metal–Organic Frameworks as Multifunctional Solid Catalysts. *Trends Chem.* **2020**, *2*, 454–466. [CrossRef]
55. Furukawa, H.; Cordova, K.E.; Yaghi, O.M. The chemistry and applications of metal-organic frameworks. *Science* **2013**, *341*, 974–986. [CrossRef]
56. Lee, J.; Farha, O.K.; Roberts, J.; Scheidt, K.A.; Nguyen, S.T.; Hupp, J.T. Metal–organic framework materials as catalysts. *Chem. Soc. Rev.* **2009**, *38*, 1450–1459. [CrossRef]
57. Wang, Q.; Astruc, D. State of the Art and Prospects in Metal–Organic Framework (MOF)-Based and MOF-Derived Nanocatalysis. *Chem. Rev.* **2020**, *120*, 1438–1511. [CrossRef]
58. Park, K.S.; Ni, Z.; Cote, A.P.; Choi, J.Y.; Huang, R.D.; Uribe-Romo, F.J.; Chae, H.K.; O'Keeffe, M.; Yaghi, O.M. Exceptional chemical and thermal stability of zeolitic imidazolate frameworks. *Proc. Natl. Acad. Sci. USA* **2006**, *103*, 10186–10191. [CrossRef] [PubMed]
59. Wang, H.; Pei, X.; Kalmutzki, M.J.; Yang, J.; Yaghi, O.M. Large Cages of Zeolitic Imidazolate Frameworks. *Acc. Chem. Res.* **2022**, *55*, 707–721. [CrossRef]
60. Na, K.; Choi, M.; Yaghi, O.M.; Somorjai, G.A. Metal Nanocrystals Embedded in Single Nanocrystals of MOFs Give Unusual Selectivity as Heterogeneous Catalysts. *Nano Lett.* **2014**, *14*, 5979–5983. [CrossRef]
61. Rungtaweevoranit, B.; Baek, J.; Araujo, J.R.; Archanjo, B.S.; Choi, K.M.; Yaghi, O.M.; Somorjai, G.A. Copper Nanocrystals Encapsulated in Zr-based Metal–Organic Frameworks for Highly Selective CO_2 Hydrogenation to Methanol. *Nano Lett.* **2016**, *16*, 7645–7649. [CrossRef] [PubMed]
62. Michaud, P.; Astruc, D.; Ammeter, J.H. Electron-transfer pathways in the reduction of d6 and d7 organoiron cations by lithium tetrahydroaluminate and sodium tetrahydroborate. *J. Am. Chem. Soc.* **1982**, *104*, 3755–3757. [CrossRef]
63. Wang, C.; Tuminetti, J.; Wang, Z.; Zhang, C.; Ciganda, R.; Moya, S.; Ruiz, J.; Astruc, D. Hydrolysis of Ammonia-Borane over Ni/ZIF-8 Nanocatalyst: High Efficiency, Mechanism, and Controlled Hydrogen Release. *J. Am. Chem. Soc.* **2017**, *139*, 11610–11615. [CrossRef]
64. Fu, F.; Wang, C.; Wang, Q.; Martinez-Villacorta, A.M.; Escobar, A.; Chong, H.; Wang, X.; Moya, S.; Salmon, L.; Fouquet, E.; et al. Highly Selective and Sharp Volcano-type Synergistic Ni_2Pt@ZIF-8-Catalyzed Hydrogen Evolution from Ammonia Borane Hydrolysis. *J. Am. Chem. Soc.* **2018**, *140*, 10034–10042. [CrossRef]
65. Wang, C.; Liu, X.; Wu, Y.; Astruc, D. PtNi@ZIF-8 nanocatalyzed high efficiency and complete hydrogen generation from hydrazine borane: Origin and mechanistic insight. *J. Mater. Chem. A* **2022**, *10*, 17614–17623. [CrossRef]
66. Kang, N.; Wei, X.; Shen, R.; Li, B.; Guisasola, E.; Cal, E.; Moya, S.; Salmon, L.; Wang, C.; Coy, E.; et al. Fast Au-Ni@ZIF-8-catalyzed ammonia borane hydrolysis boosted by dramatic volcano-type synergy and plasmonic acceleration. *Appl. Catal. B* **2023**, *320*, 121957. [CrossRef]
67. Zhao, Q.; Liu, X.; Astruc, D. Tetrahydroxydiboron (bis-boric acid), a versatile reagent for borylation, hydrogenation, catalysis, radical reactions and H_2 generation. *Eur. J. Inorg. Chem.* **2023**. [CrossRef]
68. Hou, C.-C.; Li, Q.; Wang, C.-J.; Peng, C.-Y.; Chen, Q.-Q.; Ye, H.-F.; Fu, W.-F.; Che, C.-M.; López, N.; Chen, Y. Ternary Ni–Co–P nanoparticles as noble-metal-free catalysts to boost the hydrolytic dehydrogenation of ammonia-borane. *Energy Environ. Sci.* **2017**, *10*, 1770–1776. [CrossRef]
69. Sun, D.; Hao, Y.; Wang, C.; Zhang, X.; Yu, X.; Yang, X.; Li, L.; Lu, Z.; Shang, W. TiO_2–CdS supported CuNi nanoparticles as a highly efficient catalyst for hydrolysis of ammonia borane under visible-light irradiation. *Int. J. Hydrogen Energy* **2020**, *45*, 4390–4402. [CrossRef]
70. Wang, Q.; Fu, F.; Yang, S.; Martinez Moro, M.; Ramirez, M.; Moya, S.; Salmon, L.; Ruiz, J.; Astruc, D. Dramatic Synergy in CoPt Nanocatalysts Stabilized by "Click" Dendrimers for Evolution of Hydrogen from Hydrolysis of Ammonia Borane. *ACS Catal.* **2019**, *9*, 1110–1119. [CrossRef]
71. Linic, S.; Aslam, U.; Boerigter, C.; Morabito, M. Photochemical transformations on plasmonic metal nanoparticles. *Nat. Mater.* **2015**, *14*, 567–576. [CrossRef] [PubMed]
72. Wang, C.; Astruc, D. Nanogold plasmonic photocatalysis for organic synthesis and clean energy conversion. *Chem. Soc. Rev.* **2014**, *43*, 7188–7216. [CrossRef]
73. Gellé, A.; Jin, T.; de la Garza, L.; Price, G.D.; Besteiro, L.V.; Moores, A. Applications of Plasmon-Enhanced Nanocatalysis to Organic Transformations. *Chem. Rev.* **2020**, *120*, 986–1041. [CrossRef] [PubMed]
74. Zada, A.; Muhammad, P.; Ahmad, W.; Hussain, Z.; Ali, S.; Khan, M.; Khan, Q.; Maqbool, M. Surface Plasmonic-Assisted Photocatalysis and Optoelectronic Devices with Noble Metal Nanocrystals: Design, Synthesis, and Applications. *Adv. Funct. Mater.* **2019**, *30*, 1906744. [CrossRef]
75. Wen, M.; Kuwahara, Y.; Mori, K.; Yamashita, H. Enhancement of Catalytic Activity Over AuPd Nanoparticles Loaded Metal Organic Framework Under Visible Light Irradiation. *Top. Catal.* **2016**, *59*, 1765–1771. [CrossRef]
76. Rej, S.; Hsia, C.-F.; Chen, T.-Y.; Lin, F.-C.; Huang, J.-S.; Huang, M.H. Facet-Dependent and Light-Assisted Efficient Hydrogen Evolution from Ammonia Borane Using Gold–Palladium Core–Shell Nanocatalysts. *Angew. Chem. Int. Ed.* **2016**, *55*, 7222–7226. [CrossRef]
77. Verma, P.; Yuan, K.; Kuwahara, Y.; Mori, K.; Yamashita, H. Enhancement of plasmonic activity by Pt/Ag bimetallic nanocatalyst supported on mesoporous silica in the hydrogen production from hydrogen storage material. *Appl. Catal. B* **2018**, *223*, 10–15. [CrossRef]

78. Kang, N.; Wang, Q.; Djeda, R.; Wang, W.; Fu, F.; Martinez Moro, M.; Ramirez, M.A.S.; Moya, E.; Coy, L.; Salmon, J.-L.; et al. Visible-Light Acceleration of H_2 Evolution from Aqueous Solutions of Inorganic Hydrides Catalyzed by Gold-Transition-Metal Nanoalloys. *ACS Appl. Mater. Interfaces* **2020**, *12*, 53816–53826. [CrossRef]
79. Zhang, Y.C.; He, S.; Guo, W.X.; Hu, Y.; Huang, J.W.; Mulcahy, J.R.; Wei, D. Surface-Plasmon-Driven Hot Electron Photochemistry. *Chem. Rev.* **2018**, *118*, 2927–2954. [CrossRef]
80. Zhang, P.; Wang, T.; Gong, J.L. Mechanistic Understanding of the Plasmonic Enhancement for Solar Water Splitting. *Adv. Mater.* **2015**, *27*, 5328–5342. [CrossRef]
81. Kalidindi, S.B.; Sanyal, U.; Jagirdar, B.R. Nanostructured Cu and Cu@Cu_2O core shell catalysts for hydrogen generation from ammonia–borane. *Phys. Chem. Chem. Phys.* **2008**, *10*, 5870–5874. [CrossRef]
82. Kalidindi, S.B.; Vernekar, A.A.; Jagirdar, B.R. Co–Co_2B, Ni–Ni_3B and Co–Ni–B nanocomposites catalyzed ammonia–borane methanolysis for hydrogen generation. *Phys. Chem. Chem. Phys.* **2009**, *11*, 770–775. [CrossRef] [PubMed]
83. Sun, D.H.; Li, P.Y.; Xu, Y.; Huang, J.L.; Li, Q. Monodisperse AgPd alloy nanoparticles as a highly active catalyst towards the methanolysis of ammonia borane for hydrogen generation. *RSC Adv.* **2016**, *6*, 105940–105947. [CrossRef]
84. Li, X.; Zhang, C.; Luo, M.; Yao, Q.; Lu, Z.-H. Ultrafine Rh nanoparticles confined by nitrogen-rich covalent organic frameworks for methanolysis of ammonia borane. *Inorg. Chem. Front.* **2020**, *7*, 1298–1306. [CrossRef]
85. Li, X.; Yao, Q.; Li, Z.; Li, H.; Zhu, Q.-L.; Lu, Z.-H. Modulation of Cu and Rh single-atoms and nanoparticles for high-performance hydrogen evolution activity in acidic media. *J. Mater. Chem. A* **2021**, *10*, 326–336. [CrossRef]
86. Luo, W.; Cheng, W.; Hu, M.; Wang, Q.; Cheng, X.; Zhang, Y.; Wang, Y.; Gao, D.; Bi, J.; Fan, G. Ultrahigh Catalytic Activity of l-Proline-Functionalized Rh Nanoparticles for Methanolysis of Ammonia Borane. *ChemSusChem* **2019**, *12*, 535–541. [CrossRef] [PubMed]
87. Caner, N.; Yurderi, M.; Bulut, A.; Kanberoglu, G.S.; Kaya, M.; Zahmakiran, M. Chromium based metal-organic framework MIL-101 decorated palladium nanoparticles for the methanolysis of ammonia-borane. *New J. Chem.* **2020**, *44*, 12435–12439. [CrossRef]
88. Li, H.; Yao, Z.; Wang, X.; Zhu, Y.; Chen, Y. Review on Hydrogen Production from Catalytic Ammonia Borane Methanolysis: Advances and Perspectives. *Energy Fuels* **2022**, *36*, 11745–11759. [CrossRef]
89. Özkar, S. Transition metal nanoparticle catalysts in releasing hydrogen from the methanolysis of ammonia borane. *Int. J. Hydrogen Energy* **2020**, *45*, 7881–7891. [CrossRef]
90. Yurderi, M.; Bulut, A.; Ertas, İ.E.; Zahmakiran, M.; Kaya, M. Supported copper–copper oxide nanoparticles as active, stable and low-cost catalyst in the methanolysis of ammonia–borane for chemical hydrogen storage. *Appl. Catal. B* **2015**, *165*, 169–175. [CrossRef]
91. Tunc, N.; Rakap, M. Preparation and characterization of Ni-M (M: Ru, Rh, Pd) nanoclusters as efficient catalysts for hydrogen evolution from ammonia borane methanolysis. *Renew. Energy* **2020**, *155*, 1222–1230. [CrossRef]
92. Zhang, S.; Li, M.; Li, L.; Dushimimana, F.; Zhao, J.; Wang, S.; Han, J.; Zhu, X.; Liu, X.; Ge, Q.F.; et al. Visible-Light-Driven Multichannel Regulation of Local Electron Density to Accelerate Activation of O-H and B-H Bonds for Ammonia Borane Hydrolysis. *ACS Catal.* **2020**, *10*, 14903–14915. [CrossRef]
93. Kang, N.; Shen, R.; Li, B.; Fu, F.; Espuche, B.; Moya, S.; Salmon, L.; Pozzo, J.-L.; Astruc, D. Dramatic acceleration by visible light and mechanism of AuPd@ZIF-8-catalyzed ammonia borane methanolysis for efficient hydrogen production. *J. Mater. Chem. A* **2023**, *11*, 5245–5256. [CrossRef]
94. Jo, S.; Verma, P.; Kuwahara, Y.; Mori, K.; Choi, W.; Yamashita, H. Enhanced hydrogen production from ammonia borane using controlled plasmonic performance of Au nanoparticles deposited on TiO_2. *J. Mater. Chem. A* **2017**, *5*, 21883–21892. [CrossRef]
95. Ashby, C.; Dobbs, F.R.; Harry Hopkins, P.J., Jr. Composition of lithium aluminum hydride, lithium borohydride, and their alkoxy derivatives in ether solvents as determined by molecular association and conductance studies. *J. Am. Chem. Soc.* **1975**, *97*, 3158–3162. [CrossRef]
96. Yang, X.F.; Wang, A.Q.; Qiao, B.T.; Li, J.; Liu, J.Y.; Zhang, T. Single-Atom Catalysts: A New Frontier in Heterogeneous Catalysis. *Acc. Chem. Res.* **2013**, *46*, 1740–1748. [CrossRef]
97. Liu, L.C.; Corma, A. Metal Catalysts for Heterogeneous Catalysis: From Single Atoms to Nanoclusters and Nanoparticles. *Chem. Rev.* **2018**, *118*, 4981–5079. [CrossRef] [PubMed]
98. Liang, L.; Qin, F.; Wang, S.; Wu, J.; Li, R.; Wang, Z.; Ren, M.; Liu, D.; Wang, D.; Astruc, D. Overview of the materials design and sensing strategies of nanopore devices. *Coord. Chem. Rev.* **2023**, *478*, 214998. [CrossRef]
99. Ouyang, L.Z.; Ouyang, J.; Chen, K.; Zhu, M.; Liu, Z.W. Hydrogen Production via Hydrolysis and Alcoholysis of Light Metal-Based Materials: A Review. *Nano-Micro Lett.* **2021**, *13*, 134. [CrossRef]
100. Wang, J.; Gao, Y.; Kong, H.; Kim, J.; Choi, S.; Ciucci, F.; Hao, Y.; Yang, S.H.; Shao, Z.P.; Lim, J. Non-precious-metal catalysts for alkaline water electrolysis: Operando characterizations, theoretical calculations, and recent advances. *Chem. Soc. Rev.* **2020**, *49*, 9154–9196. [CrossRef]